High coercivity in large exchange-bias Co/CoO-MgO nano-granular films*

Ge Chuan-Nan(葛传楠)[a)b)], Wan Xian-Gang(万贤纲)[a)†], Eric Pellegrin[c)], Hu Zhi-Wei(胡志伟)[d)], Wen-I Liang[e)], Michael Bruns[f)], Zou Wen-Qin(邹文琴)[a)], and Du You-Wei(都有为)[a)]

[a)] *National Laboratory of Solid State Microstructures and Department of Physics, Nanjing University, Nanjing* 210093, *China*
[b)] *Department of Physics, Jiangsu Second Normal University, Nanjing* 210013, *China*
[c)] *CELLS-ALBA Synchrotron Radiation Facility, Carretera BP* 1413, *km* 3.3, *Cerdanyola del Vallès (Barcelona) E*-08290, *Spain*
[d)] *Max Planck Institute for Chemical Physics of Solids, Nöthnitzer Straße* 40, *Dresden D*-01187, *Germany*
[e)] *Lawrence Berkeley National Lab Materials Science Division, Haimei Zheng laboratory, Berkeley CA* 94720, *USA*
[f)] *Institute for Applied Materials (IAM), Karlsruhe Institute of Technology (KIT), Hermann-von-Helmholtz-Platz* 1, *Eggenstein-Leopoldshafen D*-76344, *Germany*

(Received 25 September 2014; revised manuscript received 27 October 2014; published online 19 January 2015)

We present a detailed study on the magnetic coercivity of Co/CoO-MgO core-shell systems, which exhibits a large exchange bias due to an increase of the uncompensated spin density at the interface between the CoO shell and the metallic Co core by replacing Co by Mg within the CoO shell. We find a large magnetic coercivity of 7120 Oe around the electrical percolation threshold of the Co/CoO core/shell particles, while samples with a smaller or larger Co metal volume fraction show a considerably smaller coercivity. Thus, this study may lead to a route to improving the magnetic properties of artificial magnetic material in view of potential applications.

Keywords: granular films, exchange bias, coercivity

PACS: 45.70.Cc, 75.30.Et, 75.50.Vv, 75.60.Ej **DOI:** 10.1088/1674-1056/24/3/034501

1. Introduction

Magnetic nanoparticles are attractive for their potential applications in ultrahigh-density magnetic data storage.[1] The storage density can be improved by scaling down the magnetic particle size, but the magnetic ordering of particles becomes unstable as the particle size is decreased below a certain threshold which is the so-called "superparamagnetic limit".[2] Thus, finding a way to stabilize the magnetization in magnetic nanoparticles systems is of both fundamental and technological importance.

Exchange bias[3–6] (i.e., the shift of the hysteresis loop along the field axis) has been extensively studied in various systems and has been identified as an efficient method to stabilize the magnetization against thermal fluctuations.[2] Although tremendous efforts have been devoted to understanding this intriguing phenomenon, the microscopic origin of the exchange bias (EB) effect is still controversial. The generally accepted uncompensated spin scenario can reasonably well explain the EB due to the existence of pinned uncompensated spins as well as the enhanced coercive field due to the existence of rotatable uncompensated spins at the interface between antiferromagnetic (AFM)/ferromagnetic (FM).[19] Co/CoO core-shell systems typically show a high exchange bias field (H_E).[3] Moreover, since the MgO host matrix has a similar lattice parameter as compared with CoO, diluting the Co atoms within the CoO shell with non-magnetic Mg will increase the uncompensated spin density at the AFM/FM CoO/Co interface.[7] Thus, we expect to directly observe the uncompensated spins from the characteristic Co^{2+} atomic multiplet features in the Co-$L_{2,3}$ x-ray magnetic circular dichroism (XMCD) spectra, which is rarely reported in the literature. Although some intriguing correlation exists between H_E and the coercive field H_C, detailed investigations of the various factors influencing H_C are rare.[8–14] In this work, we thus provide a systematic study on the cooling field- and temperature-dependence of the magnetic coercivity in exchange bias Co/CoO-MgO nano-granular films produced on Si(100) substrates using magnetron sputtering. We find that in this system the EB plays an important role for H_C. In addition, the Co metal volume fraction has a considerable effect on both the coercivity and exchange bias and the samples near the electrical percolation threshold exhibit the largest H_C. The physical properties of granular films can thus be easily tailored by adjusting the composition, the volume fraction of constituent materials, and the preparation conditions. In addition, nano-granular films are easily fabricated. We therefore believe that this study may lead to a route to improving the above magnetic properties in view of potential applications.

*Project supported by the National Basic Research Program of China (Grant No. 2012CB932304), the National Natural Science Foundation of China (Grant Nos. U1232210, 91122035, 11174124, and 11374137), the Natural Science Foundation of the Jiangsu Higher Education Institutions of China (Grant No. 14KJB140003), and the Priority Academic Program Development of Jiangsu Higher Education Institutions, China.

†Corresponding author. E-mail: xgwan@nju.edu.cn

© 2015 Chinese Physical Society and IOP Publishing Ltd

2. Experiment

All nano-granular film samples were prepared on Si(100) substrates by magnetron sputtering with a base oxygen partial pressure of 2×10^{-7} mbar using a RF power of 140 W and a typical deposition time of one hour. The composite sputtering targets were made by adhering small square-shaped pieces of highly purified cobalt metal onto a MgO plate. All Co/CoO-MgO samples with different Co metal volume ratios were prepared at ambient temperature via sputtering from the above targets with different MgO to Co surface compositions. During the sputtering process, the outer surface of the Co particles is oxidized, thus forming the CoO shells. The ratio of Co metal to MgO surface on the sputtering targets thus determines the resulting Co metal volume composition ratio. The exact composition of all samples was investigated by energy dispersive x-ray spectroscopy (EDX).

3. Results and discussion

We have measured the room temperature resistivity data as a function of the Co metal volume ratio and we show the results in Fig. 1. The resistivity of all nano-granular film samples with identical areas and thicknesses was measured at room temperature using the four-terminal measuring technique. For metal/insulator transition-type granular films, the three typical regions which depend on the Co metal volume fraction x are the following: $x \approx x_p$, $x < x_p$, and $x > x_p$, where x_p is the percolation threshold at which the granules begin to form an electrically connected network.[15,16] As shown in Fig. 1, the percolation threshold is around 56% Co metal volume ratio, which is close to that of other granular metal films.[17] When the Co metal volume ratio is less than 56%, the Co/CoO particles are well-separated and the electron hopping between them is small. Consequently, the system shows a high resistivity and exhibits insulating behavior (see Fig. 1). By increasing the Co content, the hopping between the core/shell particles becomes increasingly possible and, consequently, the resistivity decreases. If the Co concentration is larger than the electrical percolation threshold value, an electrically connected network of particles is formed and the Co/CoO-MgO system exhibits metallic properties.

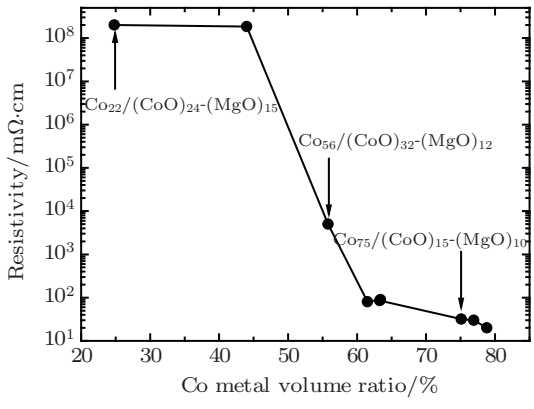


Fig. 1. Resistivity as a function of the Co metal volume ratio measured at room temperature. The samples that are discussed further in the present study are highlighted by their chemical composition.

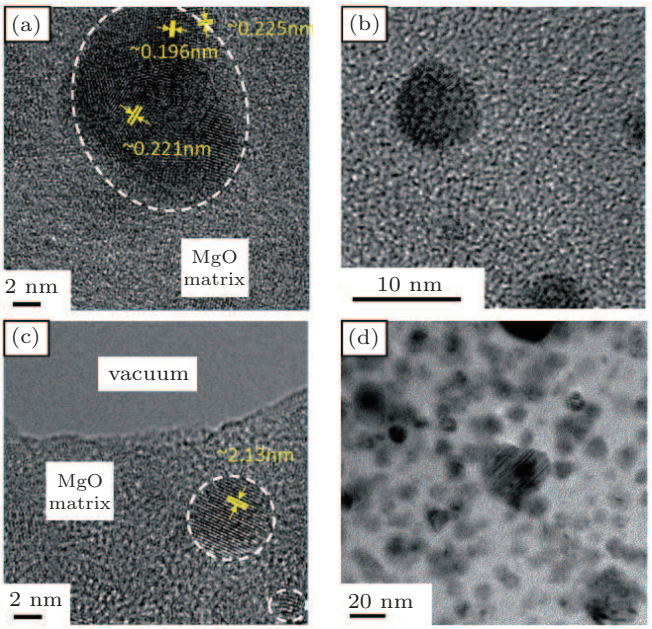


Fig. 2. (color online) High-resolution transmission electron micrographs showing the size and morphology of (a) the $Co_{22}/(CoO)_{24}$-$(MgO)_{15}$, (b) and (c) the $Co_{56}/(CoO)_{32}$-$(MgO)_{12}$, and (d) the $Co_{75}/(CoO)_{15}$-$(MgO)_{10}$ samples.

Using high-resolution transmission electron microscopy (HRTEM), we have investigated the morphology of the Co/CoO-MgO systems. In Fig. 2, high-resolution transmission electron micrographs showing the size and morphology of the sample $Co_{22}/(CoO)_{24}$-$(MgO)_{15}$ (Figs. 2(a)), the sample $Co_{56}/(CoO)_{32}$-$(MgO)_{12}$ (Figs. 2(b) and 2(c)), and the sample $Co_{75}/(CoO)_{15}$-$(MgO)_{10}$ (Fig. 2(d)). Among them there are two representative samples, one being $Co_{56}/(CoO)_{32}$-$(MgO)_{12}$ which is at the electrical percolation threshold and the other being $Co_{75}/(CoO)_{15}$-$(MgO)_{10}$ which is above the electrical percolation threshold. Small Co metal particles covered with a CoO shell can be seen that have an approximately spherical shape and that are embedded in a non-magnetic MgO matrix. The interface between the ferromagnetic (FM) Co metal core and the AFM CoO shell is irregular and roughness in these isolated particles. As shown in (Figs. 2(b) and 2(c)) for $Co_{56}/(CoO)_{32}$-$(MgO)_{12}$, these Co/CoO particles are quite separated. Increasing the Co metal volume fraction, the particles size seems to increase slightly and, more importantly, the coverage concentration of Co/CoO particles becomes larger so that the Co/CoO particles will form a connected network as is obvious from Fig. 2(d). These results are thus consistent with the existence of a percolation threshold at around 56% Co metal volume fraction. The aforementioned interface roughness between the FM core and the AFM shell as well as the small particle size in our granular films are the factors that increase the H_E in the Co/CoO-MgO granular film. Another

aspect that becomes clear from the HRTEM images shown in Fig. 2 is that the Co core of the Co/CoO core/shell exhibits a crystalline structure with a lattice spacing of about 2.13 nm similar to the lattice parameter of 2.5 nm for hcp Co. On the other hand, the MgO matrix as well as possibly the CoO shells have a non-crystalline or amorphous character as can easily be seen from the inter-granular spaces shown in Fig. 2.

In order to characterize the chemical aspects as well as the electronic and magnetic structure of the samples, we have performed Co2p x-ray photoemission spectroscopy (XPS), x-ray absorption (XAS), and x-ray magnetic circular dichroism (XMCD) measurements with the resulting data shown in Fig. 3. As can be seen from the XPS data, the Co2p lines consist of a superposition of Co metal and CoO spectra (plus the CoL_{MM} Auger line at 777 eV binding energy), giving evidence for the Co/CoO chemical structure of the core/shell nano-granules. This is corroborated by the $CoL_{2,3}$ absorption data in Fig. 3(b) the spectra taken from the $Co_{75}/(CoO)_{15}$-$(MgO)_{10}$ sample using circular polarized light with the photon spin parallel (μ^+-red line) and antiparallel (μ^--black line) with respect to an external magnetic field of 6 T. The experimental XMCD difference spectrum $\Delta\mu = \mu^+ - \mu^-$ is shown as a red line in Fig. 3(d) (red line). While the absorption spectra in Fig. 3(b) can clearly be assigned to the multiplet structures of divalent Co^{2+} as in, e.g., CoO, the difference spectrum is very similar to that of $LaCo_{0.5}Mn_{0.5}O_3$[18] in which the Co ions have a divalent state and octahedral crystal field symmetry. Simulations based on atomic crystal field multiplet calculations have been performed in order to estimate the CoO versus the Co metal contribution from the Co/CoO core/shell particles by superposing the calculated Co^{2+} spectra (Fig. 3(e)–black line) with experimental spectra from Co metal (Fig. 3(e)–purple line). The resulting simulated XMCD spectrum is shown together with the corresponding experimental spectrum in Fig. 3(d) (green and red solid lines, respectively). From the results of this simulation shown in Figs. 3(c) and 3(d), we can estimate a CoO contribution to the XMCD signal of 70%.[19] While the results from the HRTEM, XPS, and XAS/XMCD measurements confirm the basic chemical nature of the Co/CoO core/shell particles, the electron escape depth for the latter two techniques have to be taken into account, which is a few Ångstroem and a few nm for XPS and XAS, respectively. Taking the average diameter of the Co/CoO core/shell particles into account, these obviously result in an overestimation of the CoO shell contribution as compared to the Co core. Thus, while the results from the HRTEM, XPS and XAS/XMCD are useful for determining the chemical microstructure, the overall stoichiometry as determined by our EDX measurements gives a correct perspective on the sample system as a whole.

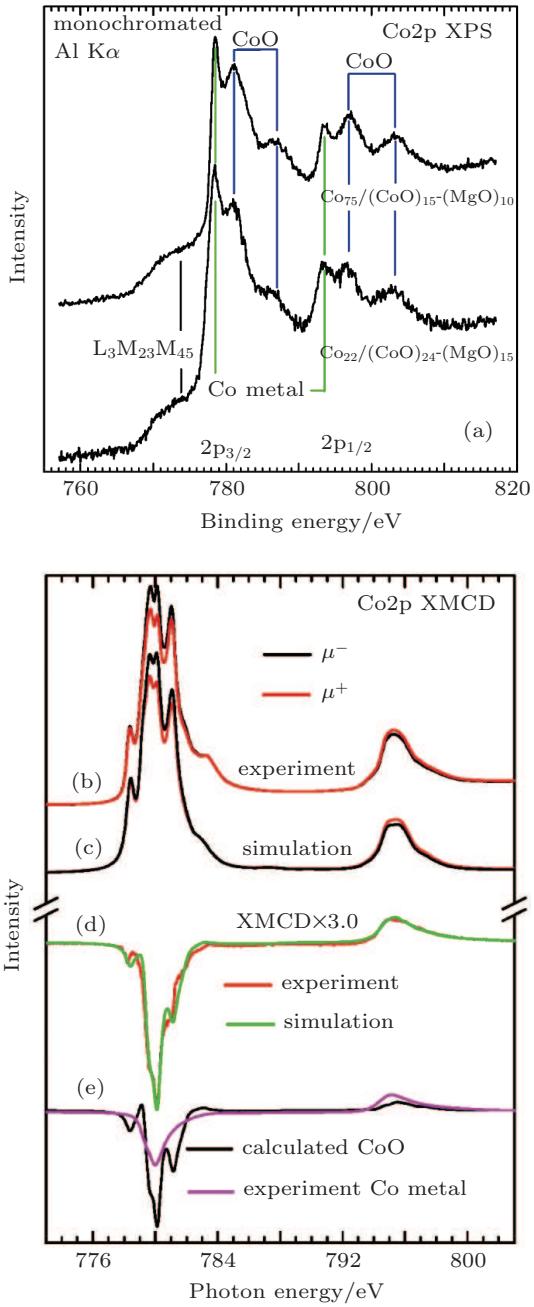


Fig. 3. (color online) (a) XPS spectra of $Co_{75}/(CoO)_{15}$-$(MgO)_{10}$ (top) and $Co_{22}/(CoO)_{24}$-$(MgO)_{15}$ (bottom). (b) Experimental μ^+ and μ^- spectra of $Co_{75}/(CoO)_{15}$-$(MgO)_{10}$. (c) Simulated μ^+ and μ^- spectra generated from a superposition of calculated data for CoO and experimental data for Co metal. (d) Comparison of the experimental XMCD spectrum of $Co_{75}/(CoO)_{15}$-$(MgO)_{10}$, and (e) the simulated XMCD spectrum by a superposition of the calculated XMCD from the CoO shell (the black line shown in panel (e)) and experimental Co metal XMCD (the magenta line shown in panel (e)).

Based on the data given in Figs. 3(b)–3(e), we have performed an evaluation of the Co2p XMCD spectra using the approximate XMCD sum rules derived by Carra *et al*. This leads to an experimental ratio of m_{orb}/m_{spin} of the Co^{2+} orbital over the spin over a magnetic moment of 0.24.[22] Going now further and using the explicit sum rules by Thole *et al*, the XMCD spectra yield for the Co^{2+} in a $m_{spin} = 2.54\mu_B$ and a $m_{orb} = 0.61\mu_B$. Table 1 gives a comparison of these figures with the corresponding values for CoO and Co metal, which

gives evidence for the large magnetic anisotropy in these samples as provided by the Co^{2+} ions.

Table 1. Overview on the spin and orbital magnetic moments for different sample systems.

	m_{spin}	m_{orb}	m_{orb}/m_{spin}
Co metal	$1.636\mu_B$	$0.154\mu_B$	0.09
CoO	$2.12\mu_B$	$0.99\mu_B$	0.47
Co/CoO-MgO	$2.54\mu_B$	$0.61\mu_B$	0.24

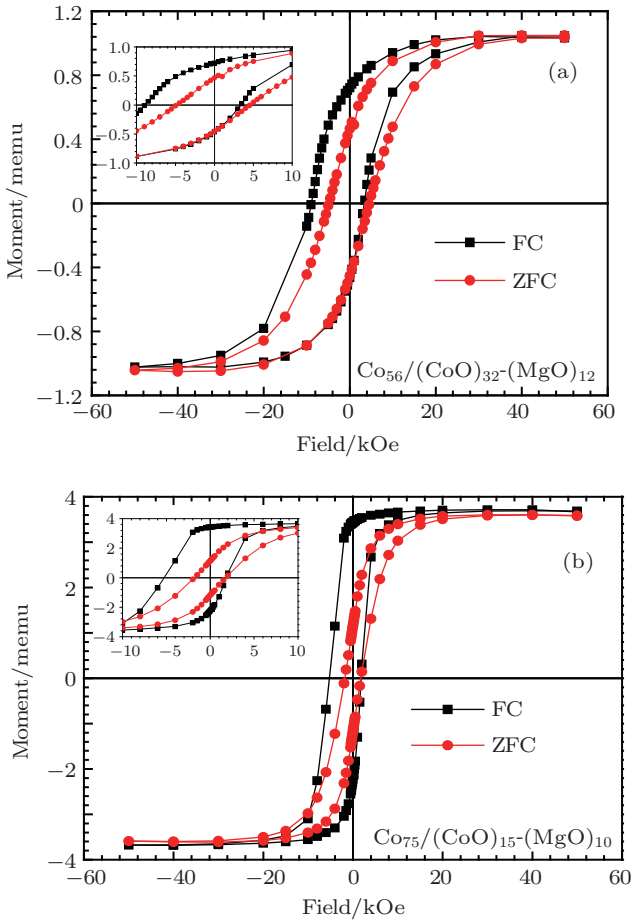


Fig. 4. (color online) Magnetic hysteresis loops of (a) the $Co_{56}/(CoO)_{32}$-$(MgO)_{12}$ sample and (b) the $Co_{75}/(CoO)_{15}$-$(MgO)_{10}$ sample measured at 2 K after cooling the samples in zero field (ZFC) or in a 5 kOe cooling field (FC), respectively. The inserts show the details of the hysteresis loops.

It is well known that magnetic granular films are good candidates to realize prominent/peculiar magnetic properties such as a large H_E and an enhanced coercivity that remarkably differ from the magnetic properties of bulk materials.[20] We thus measured the magnetic properties by using a Quantum Design superconducting quantum interference device (SQUID) magnetometer. The magnetic coercivity H_C (i.e., the half-width of the magnetic hysteresis loop) is an important parameter to characterize magnetic materials. Coercivity is a complex property that is determined by the competition among magneto-crystalline anisotropy energy (MAE), domain wall creation, and structural defects. For nanoparticles, both volume anisotropy and surface anisotropy contribute to the MAE.[21] For very small particles, the volume anisotropy is proportional to the particle volume, while the symmetry breaking at the nanoparticle surface results in the surface anisotropy.[22,23] In our granular films, the sample just at the percolation threshold has the highest ratio of surface to volume, which contributes to the MAE. Thus, it is interesting to study the effect of the Co metal volume fraction on the magnetic properties. Our results show that below the percolation threshold, increasing the Co metal content will slightly enlarge the size of the Co clusters and also increase H_C and H_E. Both H_C and H_E reach the maximum around the percolation threshold. As illustrated in Fig. 4(a), the hysteresis loop for zero-field cooling (ZFC) of $Co_{56}/(CoO)_{32}$-$(MgO)_{12}$ is symmetric and does not exhibit exchange bias. The H_C of the ZFC curve is about 4784 Oe. On the other hand, the hysteresis loop under 5 kOe field cooling (FC) exhibits a clear asymmetry as compared to the ZFC data yielding a high H_E of about 2743 Oe while H_C increases to 6135 Oe. This already indicates the influence of H_E (namely the exchange coupling between the Co metal core and the CoO-MgO shell) on the size of H_C.

For comparison, the ZFC and FC magnetization curves of the $Co_{75}/(CoO)_{15}$-$(MgO)_{10}$ sample have been measured under the same conditions. From the ZFC data for $Co_{75}/(CoO)_{15}$-$(MgO)_{10}$ shown in Fig. 4(b), we obtain a H_C of only 1807 Oe, whereas the FC data yield a H_C of about 3679 Oe and a H_E of 1696 Oe. We have performed magnetization measurements for samples well below the percolation threshold and found that for these samples, both H_C and H_E are quite small. On the other hand, based on the magnetic force microscopy (MFM) measurements that we have performed on the samples above the percolation threshold, we could determine that these are multi-domain like and we thus believe that in this case, the decrease of H_C is mainly due to magnetic domain motion.

The temperature dependence of the exchange bias H_E and the coercive field H_C has also been investigated. All the magnetic hysteresis loops were measured from 2 K to 200 K after cooling in a 2 kOe field. The resulting H_E and H_C as a function of temperature for $Co_{56}/(CoO)_{32}$-$(MgO)_{12}$ and $Co_{75}/(CoO)_{15}$-$(MgO)_{10}$ samples are summarized in Fig. 5. As shown in Fig. 5, H_E decreases dramatically as the temperature increases and vanishes at about 200 K. The thermal dependence of H_E reflects the thermal dependence of the pinned uncompensated spins of the CoO shell at the interface with the Co metal core.[24] On the other hand, the coercive field H_C decreases as temperature increases due to superparamagnetism.[25] It is interesting to see that for both samples, the temperature behavior of H_C is quite similar to that of H_E, which also indicates the contribution of the exchange bias to the enhancement of H_C.

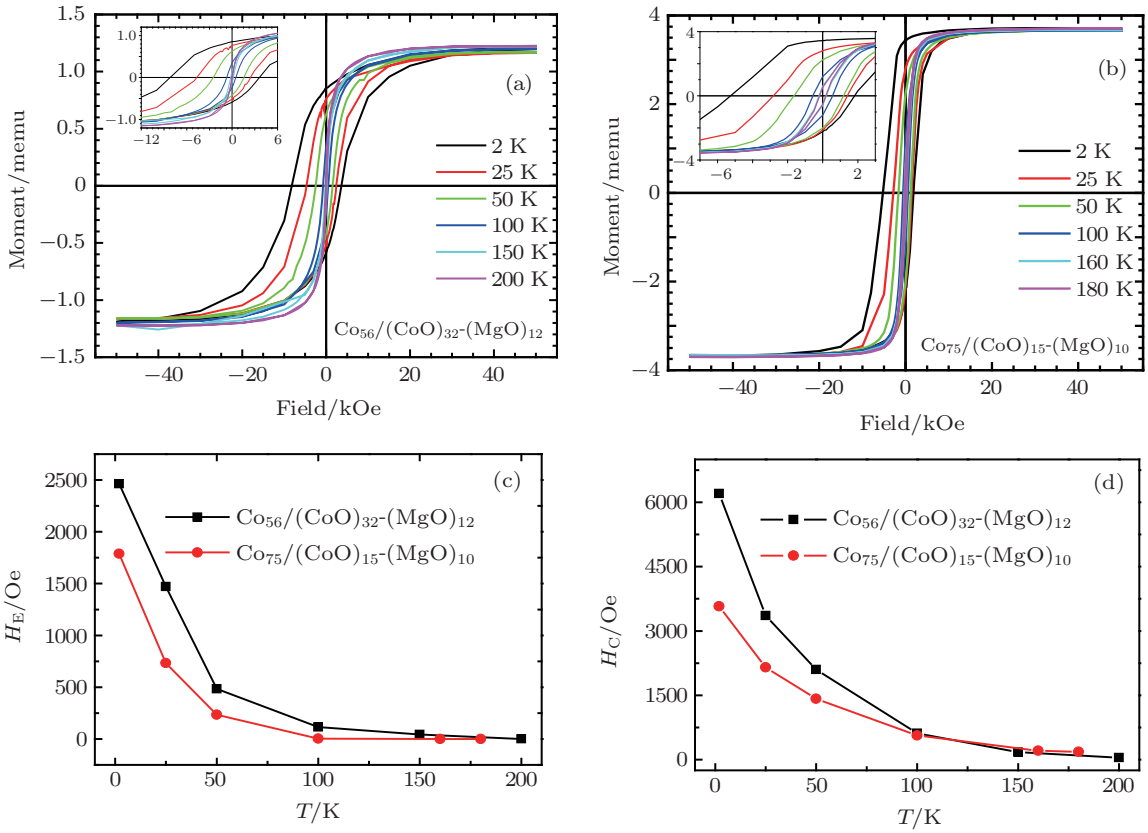


Fig. 5. (color online) Magnetic hysteresis loops of (a) the $Co_{56}/(CoO)_{32}$-$(MgO)_{12}$ sample and (b) the $Co_{75}/(CoO)_{15}$-$(MgO)_{10}$ sample. All data were taken by warming up after cooling down to 2 K in a 2 kOe field. The inserts show the details of the hysteresis loops. (c) Exchange bias H_E as a function of temperature for the $Co_{56}/(CoO)_{32}$-$(MgO)_{12}$ sample and the $Co_{75}/(CoO)_{15}$-$(MgO)_{10}$ sample. (d) Magnetic coercive field H_C as a function of temperature for the $Co_{56}/(CoO)_{32}$-$(MgO)_{12}$ sample and the $Co_{75}/(CoO)_{15}$-$(MgO)_{10}$ sample.

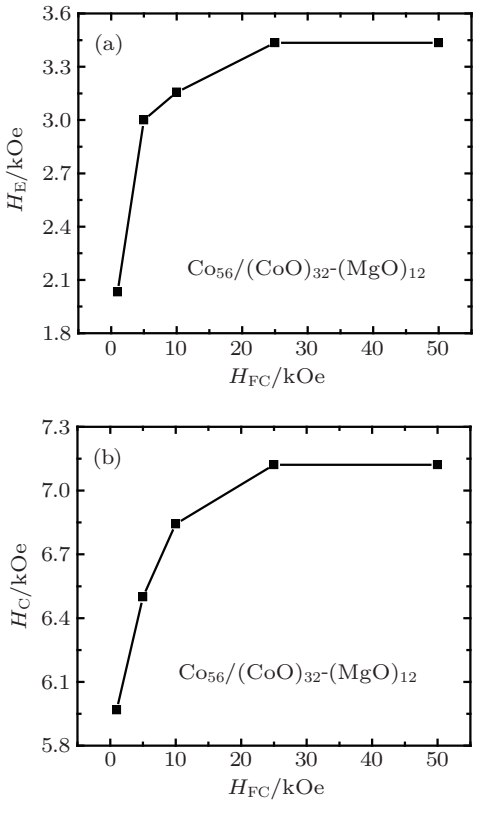


Fig. 6. (a) Exchange bias H_E and (b) coercive field H_C as functions of the cooling field H_{FC} for $Co_{56}/(CoO)_{32}$-$(MgO)_{12}$ measured after cooling the sample down to 2 K.

We investigated the dependence of H_E and H_C on the cooling field H_{FC} and the results from the $Co_{56}/(CoO)_{32}$-$(MgO)_{12}$ sample are shown in Fig. 6. The SQUID hysteresis loops were measured in the -5 T to $+5$ T range after cooling from room temperature down to 2 K in various cooling fields ($H_{FC} = 1$ kOe to 50 kOe). As the sample is cooled through T_N, the AFM surface spins of the CoO shell couple to the external magnetic cooling field H_{FC}. H_{FC} thus modifies the AFM surface spin structure and will possibly enlarge the uncompensated magnetic moment.[26,27] Thus, as shown in Fig. 6, both H_C and H_E increase almost logarithmically with increasing cooling field. The uncompensated spins do saturate at a high H_{FC} value of about 2.5 T. Consequently, when H_{FC} is above 2.5 T both H_C and H_E reach their maximum values of 7121 Oe and 3435 Oe, respectively. In analogy to the findings by Domingo *et al.*,[28] for high cooling fields H_C saturates while the H_E slightly decreases as shown in Fig. 6.

4. Conclusion

In conclusion, a quite large coercive field H_C of about 7121 Oe and an exchange bias H_E of about 3435 Oe are achieved in the $Co_{56}/(CoO)_{32}$-$(MgO)_{12}$ samples which is located right at an electrical percolation threshold. The ferro-

magnetic XMCD signal from the nominally AFM CoO shell yields the existence of rotatable uncompensated Co^{2+} spins. From the temperature-dependence of both H_C and H_E we could derive a strong functional dependence between the underlying pinned and rotatable uncompensated spins. Thus, the exchange bias systems based on Co/CoO-MgO nano-granular films may provide a way to tune the behavior of magnetic storage devices and provide new possibilities for improving the magnetic properties of exchange bias-based magnetic devices.

Acknowledgment

XMCD experiments were performed at the BL29 Boreas beamline of the ALBA Synchrotron Light Facility with the collaboration of ALBA staff.

References

[1] Nogués J, Sort J, Langlais V, Skumryeva V, Suriñach S, Muñoz J S and Baró M D 2005 *Phys. Rep.* **422** 65
[2] Skumryev V, Stoyanov S, Zhang Y, Hadjipanayis G, Givord D and Nogués J 2003 *Nature* **423** 850
[3] Meiklejohn W H and Bean C P 1956 *Phys. Rev.* **102** 1413
[4] Cheng Z H, Luo Y and Zhao G P 2013 *Acta Phys. Sin.* **62** 176102 (in Chinese)
[5] Zhang H W, Zhou W P and Liu E K 2013 *Acta Phys. Sin.* **62** 147501 (in Chinese)
[6] Shi Z, Du J and Zhou S M 2014 *Chin. Phys. B* **23** 027503
[7] Hong J I, Leo T, Smith D J and Berkowitz A E 2006 *Phys. Rev. Lett.* **96** 117204
[8] Nogués J, Leighton C and Schuller I K 2000 *Phys. Rev. B* **61** 1315
[9] Sort J, Suriñach S, Muñoz J S, Baró M D, Nogués J, Chouteau G, Skumryev V and Hadjipanayis G C 2002 *Phys. Rev. B* **65** 174420
[10] Ohldag H, Scholl A, Nolting F, Arenholz E, Maat S, Young A T, Carey M and Stöhr J 2003 *Phys. Rev. Lett.* **91** 017203
[11] Sort J, Nogués J, Amils X, Suriñach S, Muñoz J S and Baró M D 1999 *Appl. Phys. Lett.* **75** 3177
[12] Sort J, Langlais V, Doppiu S, Dieny B, Suriñach S, Muñoz J S, Baró M D, Laurent Ch and Nogués J 2004 *Nanotechnology* **15** 211
[13] Sort J, Nogués J, Suriñach S, Muñoz J S, Baró M D, Chappel E, Dupont F and Chouteau G 2001 *Appl. Phys. Lett.* **79** 1142
[14] Hou Z P, Su F and Wang W Q 2014 *Acta Phys. Sin.* **63** 087501 (in Chinese)
[15] Xiao G and Chien C L 1988 *J. Appl. Phys.* **63** 4252
[16] Zheng N, Abdul Q and Ram C 2011 *Chin. Phys. Lett.* **28** 098301
[17] Abeles B, Sheng P, Coutts M D and Arie Y 1975 *Adv. Phys.* **24** 407
[18] Burnus T, Hu Z, Hsieh H H, Joly V L J, Joy P A, Haverkort M W, Wu H, Tanaka A, Lin H J, Chen C T and Tjeng L H 2008 *Phys. Rev. B* **77** 125124
[19] Ge C, Wan X, Pellegrin E, Hu Z, Valvidares M, Barla A, Liang W I, Chu Y H, Zou W and Du Y 2013 *Nanoscale* **5** 10236
[20] Nakagawa T, Takagi Y and Yokoyama T 2012 *Phys. Rev. B* **86** 144418
[21] Tamion A, Raufast C, Hillenkamp M, Bonet E, Jouanguy J, Canut B, Bernstein E, Boisron O, Wernsdorfer W and Dupuis V 2010 *Phys. Rev. B* **81** 144403
[22] Jamet M, Wernsdorfer W, Thirion C, Mailly D, Dupuis V, Mélinon P and Pérez A 2001 *Phys. Rev. Lett.* **86** 4767
[23] Rusponi S, Cren T, Weiss N, Epple M, Buluschek P, Claude L and Brune H 2003 *Nat. Mater.* **2** 546
[24] Del Bianco L , Boscherini F, Fiorini A L, Tamisari M, Spizzo F, Vittori A M and Piscopiello E 2008 *Phys. Rev. B* **77** 094408
[25] Gittleman J I, Abeles B and Bozowski S 1974 *Phys. Rev. B* **9** 3891
[26] Leighton C, Nogueś J, Joïsson-Åkerman B J and Schuller I K 2000 *Phys. Rev. Lett.* **84** 3466
[27] Nogués J, Lederman D, Moran T J and Schuller I K 1996 *Phys. Rev. Lett.* **76** 4624
[28] Domingo N, Testa A M, Fiorani D, Binns C, Baker S and Tejada J 2007 *J. Magn. Magn. Mater.* **316** 155